Available online at www.sciencedirect.com
ScienceDirect
Materials Research Bulletin 43 (2008) 394–400
Materials Research Bulletin
www.elsevier.com/locate/matresbu

Neutron diffraction texture analysis and thermoelectric properties of BiCaCoO misfit compounds

E. Guilmeau [a,*], M. Pollet [b], D. Grebille [a], D. Chateigner [a], B. Vertruyen [c], R. Cloots [c], R. Funahashi [d], B. Ouladiaff [e]

[a] *CRISMAT-ENSICAEN Laboratory, UMR CNRS 6508, 6 Bd. Maréchal Juin, 14050 Caen Cedex, France*
[b] *Institut de Chimie de la Matière Condensée de Bordeaux (ICMCB)-CNRS, Université de Bordeaux 1, 87 Avenue du Dr. A. Schweitzer, F-33608 PESSAC, France*
[c] *Laboratory of Structural Inorganic Chemistry, University of Liège, Chemistry Department B6, Sart-Tilman, B4000 Liège, Belgium*
[d] *National Institute of Advanced Industrial Science and Technology, Midorigaoka, Ikeda, Osaka 563-8577, Japan*
[e] *ILL, BP 156, 38042 Grenoble, France*

Received 11 December 2006; received in revised form 22 February 2007; accepted 28 February 2007
Available online 4 March 2007

Abstract

Sintered, textured and single crystal products of the layered misfit $[Bi_{0.81}CaO_2]_2[CoO_2]_{1.69}$ cobaltite have been successfully synthesized and characterized. Based on structure and texture models, the orientation distribution of the hot-forged sample was successfully analysed by neutron diffraction. The results gave a clear description of the fiber texture with *c*-axes of the plate-like grains aligned parallel to the hot-forging direction. In terms of transport properties, the decrease of the electrical resistivity according to the degree of alignment and crystallinity of the materials evidenced the important role of the texturation and the strong anisotropy existing in these misfit layered cobaltites.

Keywords: A. Ceramics; A. Inorganic compounds; A. Layered compounds; B. Crystal growth; D. Electrical properties

1. Introduction

Since the discovery of large thermoelectricity in Na_xCoO_2 [1], enthusiastic efforts have been devoted to explore new Co oxides exhibiting high thermoelectric performances, and some layered cobaltites, such as $[Ca_2CoO_3][CoO_2]_{1.62}$ and $[Bi_{0.87}SrO_2]_2[CoO_2]_{1.82}$ were found to exhibit good thermoelectric (TE) properties as well [2–4].

The crystal structure of these layered cobaltites is composed of an alternate stacking of a common conductive CdI_2-type CoO_2 layer with a two-dimensional triangular lattice and a block layer, composed of one (in Na_xCoO_2) to several insulating rock-salt-type (RS) layer (in $[Bi_{0.87}SrO_2]_2[CoO_2]_{1.82}$). Derived from Na_xCoO_2, the structure of the cobalt oxide $[Bi_{0.81}CaO_2]_2[CoO_2]_{1.69}$ consists of single hexagonal CoO_2 layers stacked with quadruple rock-salt layers composed of double [Bi–O] and [Ca–O] layers. The two RS and CoO_2 layers have common *a*- and *c*-axes, while the *b*-axis lengths of the two layers are different. This misfit system exhibits a large thermopower $TEP_{300\ K} \sim 150\ \mu V/K$ and a rather low resistivity value [5–7]. Due to its high structural anisotropy, the alignment of plate-like grains by

* Corresponding author. Tel.: +33 231451367; fax: +33 231951600.
E-mail address: emmanuel.guilmeau@ensicaen.fr (E. Guilmeau).

0025-5408/$ – see front matter © 2007 Elsevier Ltd. All rights reserved.
doi:10.1016/j.materresbull.2007.02.043

mechanical and/or chemical processes is necessary to attain macroscopic properties comparable to the intrinsic crystallographic ones. The preferential grain orientation is expected to improve the transport properties of the bulk material and to reach, if possible, the TE properties of the single crystal. It is consequently of primary importance to compare the physical properties according to the material state, *i.e.*, sintered, textured, and single crystal. We present in this paper a detailed study of the $[Bi_{0.81}CaO_2]_2[CoO_2]_{1.69}$ misfit compound, in the form of sintered, textured and single-crystal samples. We report on the control of crystallisation and texturation and on the macroscopic anisotropic thermoelectric properties.

2. Experimental

The synthesis of the different samples was carried out in several ways:

(1) The polycrystalline sample was prepared by solid-state reaction between Bi_2O_3, $CaCO_3$ and Co_3O_4 precursors. These powders were mixed by ball-milling in the compositions $Bi_2Ca_2Co_{1.69}O_x$. The powder mixture was then pelletized into cylinders (18 mm in diameter, 2 mm thick) and sintered in air at 850 °C for 50 h.
(2) The textured sample was elaborated by the hot-forging method. Sintered pellets as prepared above were manually ground and sieved (sieve aperture 80 μm). The resulting powders were cold-pressed under uniaxial pressure of 120 MPa into 20 mm × 20 mm square pellets with a thickness of 2 mm. The pellet was then placed in a hot-forging furnace between two 0.06-mm-thick gold sheets to avoid any reaction with the alumina supports. The uniaxial pressure used during heating was 6 MPa and the operating temperature was fixed at 850 °C for 20 h. The sintered and textured specimen were cut, respectively, into 3 mm × 3 mm × 10 mm and 3 mm × 0.3 mm × 10 mm rectangular bars for the transport properties measurements.
(3) Single crystals (SC) were grown by the flux method. Precursor powders of Bi_2O_3, $CaCO_3$ and Co_3O_4 were mixed with a cationic composition of Bi:Ca:Co = 2:2:2 and calcined at 850 °C for 50 h. The resulting powder was mixed and calcined again in the same conditions. The powder was then mixed with Bi_2O_3, K_2CO_3 and KCl powder (weight ratio of 3:70:10:17) and heated in an alumina crucible at 900 °C for 20 h. The temperature was cooled down to 700 °C with a rate of 2 °C/h and next furnace-cooled. The single crystal specimen analysed in the frame of the present study is shown in Fig. 1.

The structural analysis of the powder specimen was performed using X-ray diffraction (XRD) on a two-circle diffractometer (Rigaku RINT-TTR) with the Cu Kα radiation. The structure of the single crystal was analysed through a global data collection using a four-circle Bruker KappaCCD diffractometer using the Mo Kα radiation. The texture of the hot-forged sample was determined from neutron diffraction spectra. A curved position-sensitive detector coupled to a tilt angle (χ) scan allowed the whole diffraction pattern treatment in the combined Rietveld-WIMV

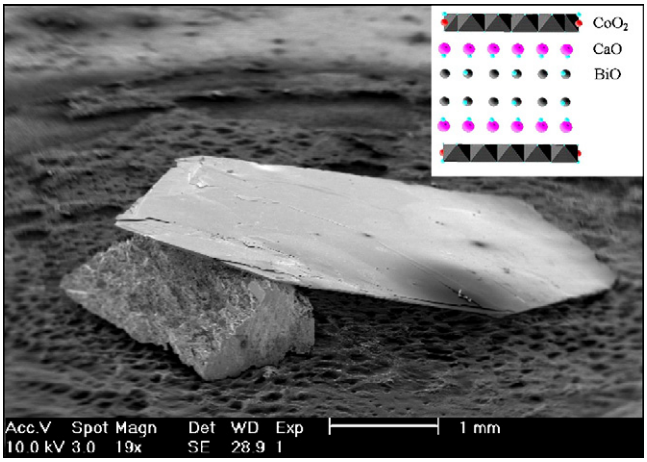

Fig. 1. SEM image of a $[Bi_{0.81}Ca_2O_4][CoO_2]_{1.62}$ single crystal. The hexagonal well-grown surface corresponds to the crystallographic *ab* planes. *Inset*: Layered crystal structure of $[Bi_{0.81}Ca_2O_4][CoO_2]_{1.69}$ misfit phase.

algorithm, implemented in the MAUD software [8]. X-ray structural determination performed on the single crystal [9,10] was used to describe the 3D structural model of the $[Bi_{0.81}CaO_2]_2[CoO_2]_{1.69}$ phase in the MAUD software using the supercell description, and to determine through an iterative methodology the texture of the cobaltite. Experiments were carried out on the D1B neutron line at the Institut Laüe Langevin, Grenoble. The neutron wavelength is monochromatised to $\lambda = 2.523$ Å. Diffracted neutrons are collected on a 80° (resolution 0.2°) 2θ range. Scans for combined analysis were operated from $\chi = 0$ to 90° (step 5°) using a fixed incidence angle ω of 25.11°. The average volume of the sample is 100 mm^3, this corresponding to measuring times around 20 min per sample orientation.

The microstructures of the specimens were observed by scanning electron microscopy (SEM). Energy and wavelength dispersive spectroscopies (EDS, WDS) were used to determine the cationic composition of the grains and single crystals. The temperature dependence of ρ was measured by a standard four-probe method using a Quantum Design PPMS system (5–300 K). Thermopower measurements were performed with an experimental setup described elsewhere [11].

3. Results and discussion

The composition of the single crystal was estimated to be $Bi_{1.62}Ca_2Co_{1.62}O_x$ whereas the grains of the sintered and textured specimens have an average composition of $Bi_{1.75}Ca_2Co_{1.65}O_x$. This is almost consistent with results reported by Leligny et al. [4]. The close compositions found on the three samples, except a slightly different Bi deficiency, prove the high stability of the cobaltite phase and mainly show that both Co and Bi layers are deficient in cations (the non-deficient composition being $Bi_2Ca_2Co_{1.69}O_x$).

Fig. 2 shows the standard θ–2θ XRD patterns of the sintered, textured, and single crystal specimens. The XRD pattern recorded for a typical $Bi_{1.62}Ca_2Co_{1.62}O_x$ single crystal is shown in Fig. 2a, where the presence of only (0 0 l)

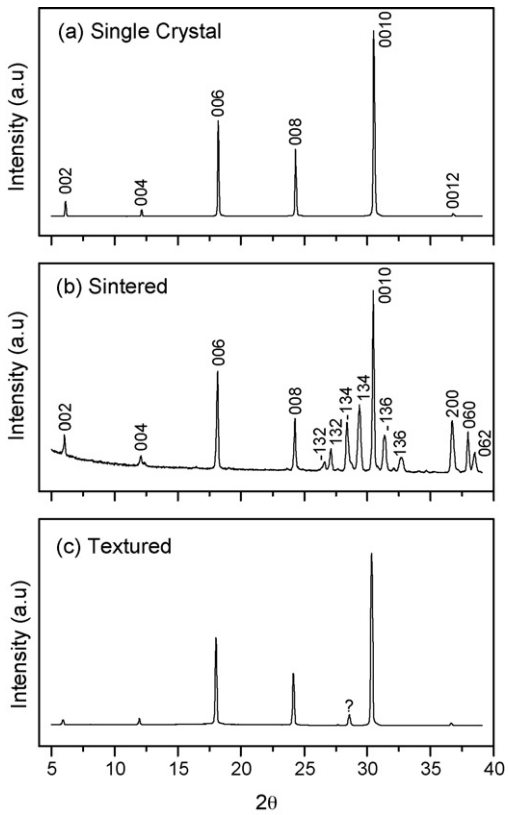

Fig. 2. XRD patterns of the: (a) single crystal, (b) sintered, and (c) textured specimens.

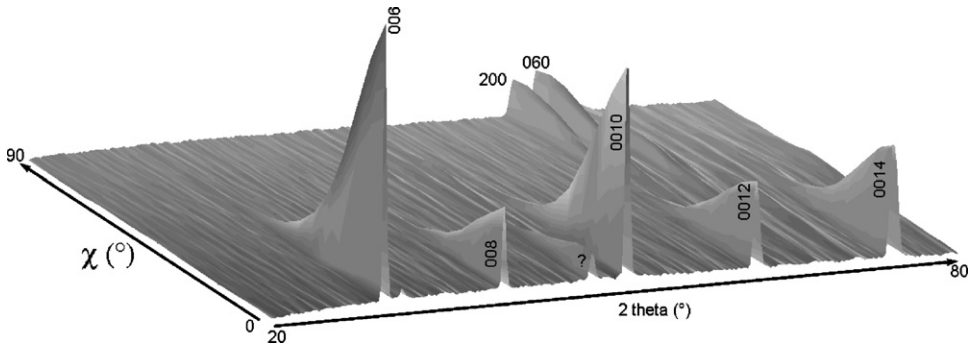

Fig. 3. Neutron diffraction pattern operated for 19 χ-scans from $\chi = 0$ to 90° (step 5°) using a fixed incidence angle ω of 25.11° ({0 0 1 0} Bragg position).

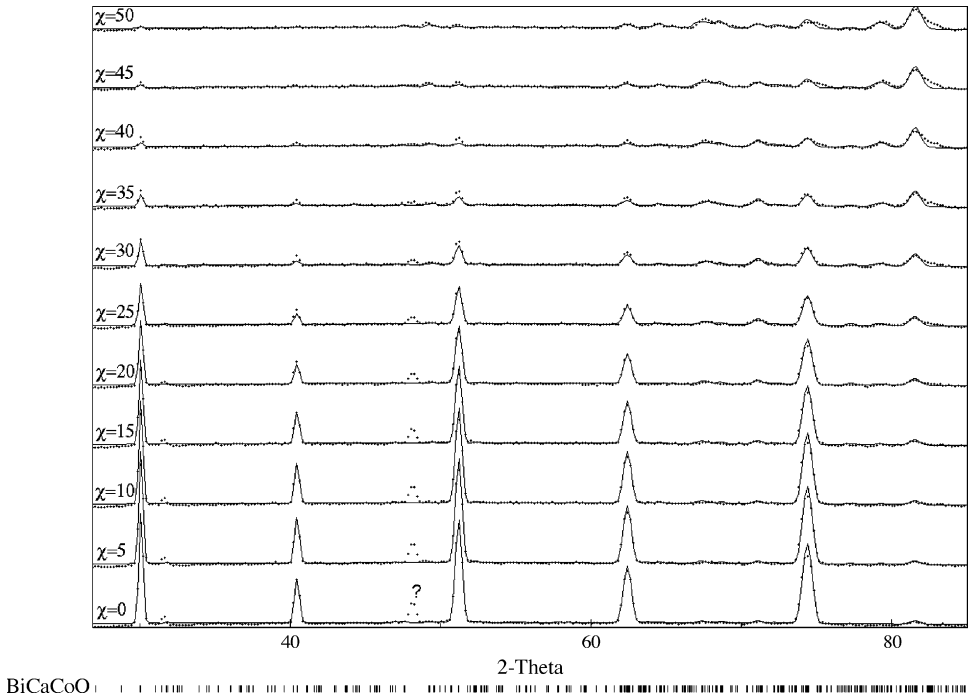

Fig. 4. 2θ experimental (dots) and calculated (lines) neutron diffraction patterns for various χ positions (0–50°). The tick marks correspond to the Bragg positions of the diffraction peaks for the $[Bi_{0.81}Ca_2O_4][CoO_2]_{1.62}$ misfit phase.

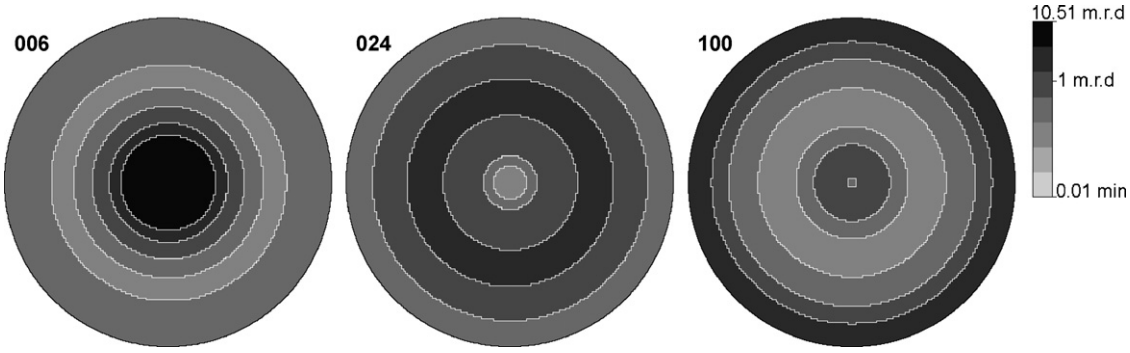

Fig. 5. {0 0 6}, {0 2 4}, and {1 0 0} pole figures recalculated from the refined orientation distribution (OD).

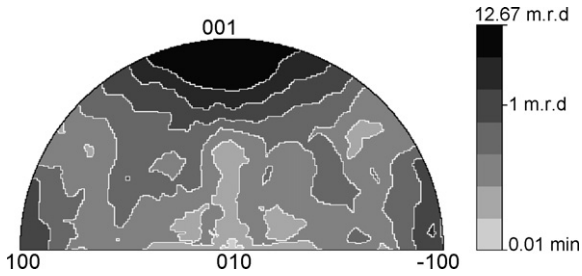

Fig. 6. Inverse pole figures calculated for the z fiber direction, parallel to the hot-forging direction.

reflections indicates that the large grown hexagonal surfaces of the crystal (Fig. 1) are the *ab*-planes. A thorough description of this complex misfit layered structure was refined using the superspace formalism would not find its place here and is detailed elsewhere [8].

On the basis of this structural model, the XRD pattern of the sintered specimen was successfully indexed (Fig. 2b). No peaks corresponding to impurity phases are observed. Fig. 2c shows the XRD pattern of the textured sample

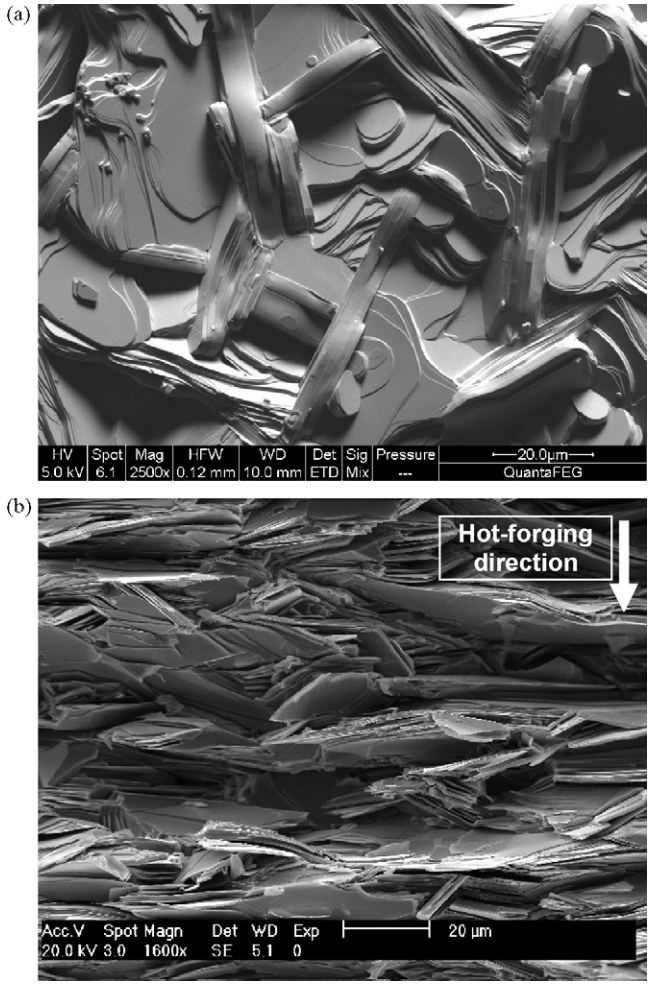

Fig. 7. SEM images of: (a) sintered and (b) textured specimens.

obtained for the surface perpendicular to the hot-forging direction. The pattern exhibits intense diffraction peaks from (0 0 *l*) crystallographic planes, indicating that the *c*-axis is preferentially oriented parallel to the hot-forging direction.

In order to calculate the orientation distribution (OD) of crystallites which defines the texture of the material, neutron diffraction was performed on the hot-forged sample. Fig. 3 shows the measured neutron diffraction pattern for all χ orientations of the sample. This graph highlights without ambiguity the (0 0 l) texture. In particular, we clearly observe the intensity decrease of the (0 0 *l*) peaks when χ increases and the appearance of the (*h k* 0) peaks when χ tends to 90°.

Based on a 3D structural model, reconstructed from the single crystal data, the whole diffraction pattern was refined. In Fig. 4, we can visually appreciate the agreement between the experimental (dots) and refined (lines) spectra for all the χ orientations, even if a diffracted peak, also observed by XRD (see '?' in Fig. 2c), has not been identified. The refinement reliability is established by RP0, RP1 for the Orientation Distribution (OD) refinement, and R_w and RB factors for the Rietveld data, equal to 6.5, 4.2, 9.6, and 6.1%, respectively.

Fig. 5 shows the {0 0 6}, {0 2 4} and {1 0 0} pole figures recalculated from the refined OD. The {0 0 6} pole figure exhibits a strong maximum for *c*-axes parallel to the sample normal. The {0 2 4} pole figure presents a small circle at the χ position around 60°, a value equal to the angle between the (0 0 6) and (0 2 4) directions in the reconstructed 3D monoclinic structure. The maximum of the distribution density around $\chi = 90°$ for the {1 0 0} pole figure is also compatible with the expected fiber texture and the structure. From the point of view of the texture development, it is really important to check which (*h k l*) planes align with their normals along the *z*-axis (normal to sample surface), which cannot be evidenced straightfully by only the pole figures in the given 2θ range. For instance, if small textural components with <*h k l*> directions (other than <0 0 *l*>) also align with the sample normal, these would not be easily visible on the pole figures of Fig. 5 themselves, though they would contain all the information. In order to visualise these eventual small components, the full representation of the OD is required, which in the case of the fiber textures can be represented by the inverse pole figures (Fig. 6) calculated for the *z* fiber direction, parallel to the hot-forging direction. It shows that the main component present in the sample is with the (0 0 l) crystallographic planes perpendicular to the hot-forging direction.

In terms of microstructure, SEM images shown in Fig. 7 highlight the texture development through the hot-forging process. The large plate-like grains, randomly oriented in the sintered sample (Fig. 7a), are stacked and aligned preferentially with their average *c*-axes parallel to the hot-forging direction (Fig. 7b).

Fig. 8 shows the temperature dependence of the electrical resistivity. In the case of the single crystal and textured specimens, the resistivity was measured along the *ab* planes and mean *ab* planes, respectively. The temperature

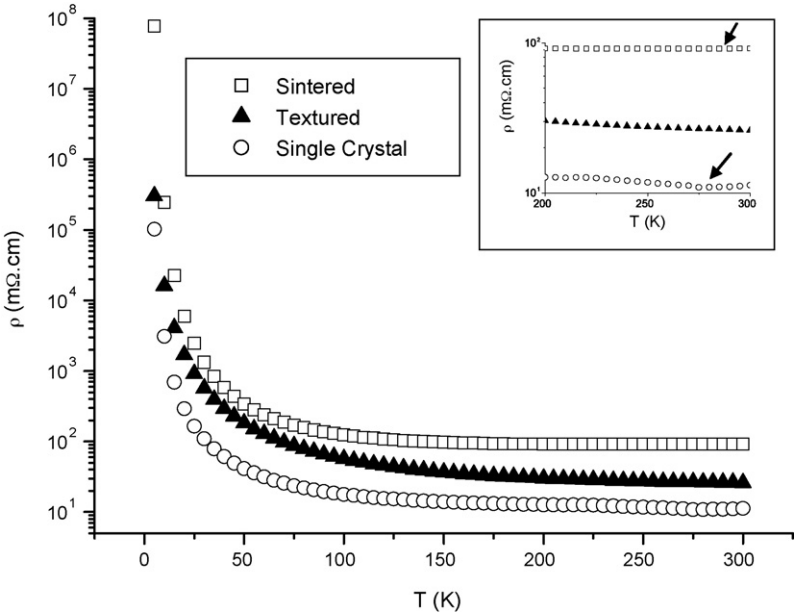

Fig. 8. Temperature dependence of the resistivity of the three specimens.

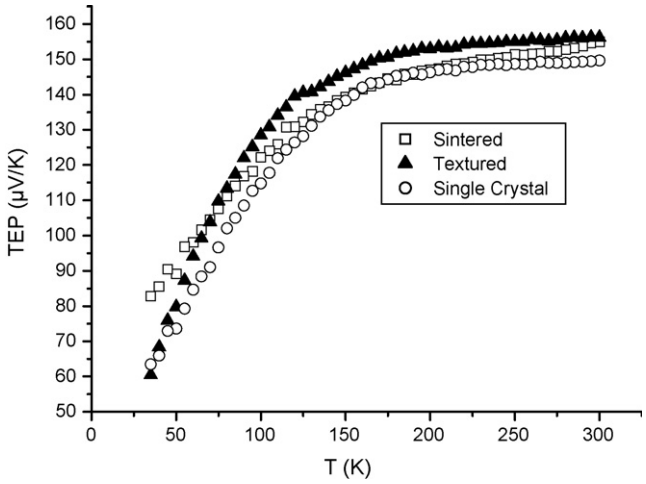

Fig. 9. Temperature dependence of the thermopower of the three specimens.

dependences show a semiconductor behavior from 5 to 250–300 K where a slight transition to a metallic state can be observed depending on the sample. The interesting point stands in the evolution of ρ according to the sample state. Whereas the sintered sample exhibits a ρ value at room temperature close to 90 mΩ cm, the hot-forged sample presents a resistivity of 26 mΩ cm, almost four times lower than the previous. The single crystal shows a resistivity of 11 mΩ cm, only two times less than the textured compound. These results highlight the strong anisotropy of the Co-based misfit layered structure and the advantage of the texture development to reduce the resistivity of the materials for optimised thermoelectric properties of potential devices.

Fig. 9 shows the thermopower of the prepared samples. The in-plane thermopower of the single crystal is 150 μV/K, and that of polycrystalline samples is about the same value. It evidences that the thermopower is not affected by the material shape, contrary to the electrical resistivity.

4. Conclusion

$[Bi_{0.81}CaO_2]_2[CoO_2]_{1.69}$ sintered, textured and single crystal products have been successfully synthesized and characterized. Based on structure and texture models, the orientation distribution of the hot-forged sample was successfully analysed by neutron diffraction. The results give a clear description of the texture and the alignment of plate-like grains with their *c*-axes parallel to the hot-forging direction. In terms of transport properties, the decrease of the resistivity according to the degree of alignment and crystallinity of the material evidences the important role of the texturation and the strong anisotropy existing in these misfit layered cobaltites.

References

[1] I. Terasaki, Y. Sasago, K. Uchinokura, Phys. Rev. B 56 (1997) R12685.
[2] R. Funahashi, I. Matsubara, H. Ikuta, T. Takeuchi, U. Mizutani, S. Sodeoka, Jpn. J. Appl. Phys. 39 (2000) L1127.
[3] A.C. Masset, C. Michel, A. Maignan, M. Hervieu, O. Toulemonde, F. Studer, B. Raveau, J. Hejtmanek, Phys. Rev. B 62 (2000) 166.
[4] H. Leligny, D. Grebille, O. Perez, A.C. Masset, M. Hervieu, B. Raveau, Acta Crystallogr. B 56 (2000) 173.
[5] A. Maignan, S. Hébert, M. Hervieu, C. Michel, D. Pelloquin, D. Khomskii, J. Phys.: Condens. Matter 15 (2003) 2711.
[6] H. Itahara, C. Xia, J. Sugiyama, T. Tani, Chem. Mater. 14 (2004) 61.
[7] E. Guilmeau, M. Mikami, R. Funahashi, D. Chateigner, J. Mater. Res. 20 (2005) 1002.
[8] D. Grebille, H. Muguerra, E. Guilmeau, H. Rousselière, R. Cloots, private communication.
[9] L. Lutterotti, S. Matthies, H.R. S Wenk, in: J.A. Szpunar (Ed.), Proceedings of the 12th International Conference on Textures of Materials, vol. 2, Montreal, NRC Research Press, 1999, pp. 1599–1604, Freeware available at: http://www.ing.unitn.it/~luttero/maud/.
[10] E. Guilmeau, D. Chateigner, J. Noudem, R. Funahashi, S. Horii, B. Ouladdiaf, J. Appl. Crystallogr. 38 (2005) 199.
[11] J. Hejmanek, Z. Jirak, M. Marysko, C. Martin, A. Maignan, M. hervieu, B. Raveau, Phys. Rev. B 60 (1999) 14057.